Molecular Dissection of Human Methionine Synthase Reductase: Determination of the Flavin Redox Potentials in Full-Length Enzyme and Isolated Flavin-Binding Domains†

Kirsten R. Wolthers, Jaswir Basran, Andrew W. Munro, and Nigel S. Scrutton*

Department of Biochemistry, University of Leicester, University Road, Leicester LE1 7RH, United Kingdom

Received December 3, 2002; Revised Manuscript Received February 4, 2003

ABSTRACT: Human methionine synthase reductase (MSR) catalyzes the NADPH-dependent reductive methylation of methionine synthase. MSR is 78 kDa flavoprotein belonging to a family of diflavin reductases, with cytochrome P450 reductase (CPR) as the prototype. MSR and its individual flavin-binding domains were cloned as GST-tagged fusion proteins for expression and purification from *Escherichia coli.* The isolated flavin domains of MSR retain UV−visible and secondary structural properties indicative of correctly folded flavoproteins. Anaerobic redox titrations on the individual domains assisted in assignment of the midpoint potentials for the high- and low-potential flavin. For the isolated FMN domain, the midpoint potentials for the oxidized/semiquinone (ox/sq) couple and semiquinone/hydroquinone (sq/hq) couple are −112 and −221 mV, respectively, at pH 7.0 and 25 °C. The corresponding couples in the isolated FAD domain are −222 mV (ox/sq) and −288 mV (sq/hq). Both flavins form blue neutral semiquinone species characterized by broad absorption peaks in the long-wavelength region during anaerobic titration with sodium dithionite. In full-length MSR, the values of the FMN couples are −109 mV (ox/sq) and −227 mV (sq/hq), and the corresponding couple values for FAD are −254 mV (ox/sq) and −291 mV (sq/hq). Separation of the MSR flavins does not perturb their thermodynamic properties, as midpoint potentials for all four couples are similar in isolated domains and in full-length MSR. The redox properties of MSR are discussed in relation to other members of the diflavin oxidoreductase family and the mechanism of electron transfer.

Methionine synthase reductase (MSR;[1] EC 2.1.1.135) is a key eukaryotic enzyme of folate and methionine metabolism where it plays a role in maintaining the activity of cobalamin-dependent methionine synthase (MS; *1*, *2*). The reaction catalyzed by MS involves methyl group transfer from methyltetrahydrofolate to homocysteine, via a cob(I)-alamin cofactor, to form methionine, tetrahydrofolate, and the intermediate methylcob(III)alamin. Over time, MS is rendered inactive owing to the oxidation of cob(I)alamin to cob(II)alamin. MSR restores MS activity through reductive methylation of cob(II)alamin using *S*-adenosylmethionine as methyl donor (*3*).

In contrast to eukaryotes, the reductive methylation of the MS cob(II)alamin cofactor in *Escherichia coli* is performed by a two-component flavoprotein system. The NADPH-dependent flavodoxin reductase [a member of the ferredoxin oxidoreductase (FNR) family] transfers reducing equivalents from NADPH to an FMN-containing flavodoxin (FLD); reduced FLD then donates an electron to MS to facilitate reductive methylation (*4*−*6*). In humans, MSR is the functional equivalent of the two-component reductase system found in *E. coli*. The primary structure of human MSR (*1*) reveals that the protein is related to cytochrome P450 reductase (CPR; *7*) and other members of the diflavin reductase family, i.e., nitric oxide synthase (NOS; *8*) and human novel reductase 1 (NR1; *9*). MSR contains two flavin-binding domains termed the NADPH/FAD-binding domain and FMN-binding domain, which are related to FNR and FLD, respectively.

Deficiencies in methionine synthesis are autosomal recessive disorders with clinical mutations mapping to the genes encoding MS or MSR (*10*, *11*). Mutations in either gene compromise the conversion of homocysteine to methionine (*12*). Elevated homocysteine levels lead to an increased risk of cardiovascular disease (*13*, *14*) and a higher incidence of neural tube defects (*15*, *16*) and Down's syndrome in newborn infants (*17*). A number of missense, nonsense, deletion, and insertion mutations have been identified in the gene encoding MSR, appearing in, and distant from, conserved putative flavin-binding regions (*18*). The interaction of a major polymorphic variant of MSR with MS is impaired and might contribute to deficiencies in methionine biosynthesis (*19*).

† This work was supported by the Lister Institute of Preventive Medicine and by a postdoctoral fellowship from the National Institutes of Health (K.R.W.). N.S.S. is a Lister Institute Research Professor.

* Corresponding author: telephone, +44 116 223 1337; fax, +44 116 252 3369; e-mail, nss4@le.ac.uk.

[1] Abbreviations: MSR, methionine synthase reductase; MS, methionine synthase; FNR, NADPH−ferredoxin oxidoreductase; FLD, flavodoxin; CPR, cytochrome P450 reductase; NOS, nitric oxide synthase; NR1, novel reductase 1; GST, glutathione *S*-transferase; ox, oxidized; sq, semiquinone; hq, hydroquinone; NHE, normal hydrogen electrode.

10.1021/bi027290b CCC: $25.00
Published on Web 03/15/2003

MSR reduces the nonphysiological electron acceptors cytochrome *c* and FeCN (*2*, *19*). Reduction rates during steady-state turnover are 25−100-fold less than those measured for NOS (*20*) and CPR (*21*) but are similar to reduction rates for human NR1 (*9*). These differences in steady-state behavior suggest key structural and/or functional differences in the electron-transfer mechanism between different members of the diflavin reductase family.

To establish both the mechanism and the thermodynamic feasibility of electron transfer, the redox potentials of the flavin cofactors were determined for MSR. The individual FAD and FMN domains were cloned from the MSR cDNA sequence for expression and purification from *E. coli*. Genetic dissection of MSR allowed us to determine the redox and spectral characteristics of the individual flavins and to evaluate whether domain separation results in perturbation of flavin properties. The flavin midpoint potentials of the isolated domains assisted in assignment of these values in full-length MSR. Previous detailed thermodynamic and stopped-flow studies of electron transfer performed on CPR (*22*−*26*), NOS (*27*−*29*), and NR1 (*30*) also assisted in evaluation of the four redox couples for MSR. This study completes the thermodynamic analysis of all known mammalian enzymes in the diflavin reductase family. Thus a thermodynamic framework is compiled for comparative analysis across the family, which will assist in the unraveling of the complex mechanisms of electron transfer in individual member proteins. It also provides a foundation for future studies of the redox properties of polymorphic variants of MSR and possible implications for methionine biosynthesis.

EXPERIMENTAL PROCEDURES

Chemicals, Media, and Enzymes. Restrictions enzymes, glutathione−Sepharose 4B, high-performance Q-Sepharose, and the plasmid pGEX-4-T1 were from Amersham Pharmacia Biotech. *Pfu* DNA polymerase was from Stratagene, and Complete protease inhibitor tablets were from Roche. NADPH and isopropyl 1-thio-β-D-galactopyranoside were from Melford Laboratories. All other chemicals were from Sigma.

Cloning of a cDNA Encoding MSR. The gene encoding MSR was initially isolated by PCR amplification from a cDNA clone (DKFZp762K116) obtained from a human melanoma cDNA library. The primers 5′ TGC CTT GAA CAT ATG AGG AGG TTT CTG TTA CTA TAT 3′ (forward primer) and 5′ GTC AAA AAA GCT GGA TCC TCT TTC TTT AAT TTC TGG 3′ (reverse primer) were designed with reference to the published sequence of the gene encoding MSR (*1*) and cloned as a *Bam*HI and *Nde*I fragment into pET15b (Novagen). High-level expression was not observed from this plasmid construct, and the opportunity was taken to replace a number of rare codons at the 5′ end of the gene by mutagenesis (Stratagene QuikChange system). The following primers were used in the mutagenesis reaction: 5′ CCG CGC GGC AGC CAT ATG CGC CGC TTT CTG CTG CTG TAT GCT ACC CAG CAG GGA CAG 3′ and 5′ CTG TCC CTG CTG GGT AGC ATA CAG CAG CAG AAA GCG GCG CAT ATG GCT GCC GCG CGG 3′. The derived gene was then amplified by PCR using the primers 5′ GTG CCG CGC GGC GAA TTC ATG CGC CGC TTT CTG CTG 3′ (forward primer) and 5′ ATC CTC TTT CTT TAA TGC GGC CGC TTA TGA CCA AAT ATC 3′ (reverse primer) and cloned into plasmid pGEX-4T-1 as an *Eco*RI and *Not*I fragment to produce plasmid pGEXMSR, which encodes a GST fusion of MSR cleavable with thrombin. Sequencing of the plasmid revealed that we obtained the genetic polymorphic variant with an isoleucine at residue 22 and a serine at position 175.

Expression Constructs for the Component FAD and FMN Domains. Plasmid constructs for the expression of the FAD domain (residues 163−698) and the FMN domain (residues 1−233) of MSR were generated by amplifying the appropriate coding sequences from the cloned cDNA by PCR using *Pfu* DNA polymerase. The constructs for the FAD and FMN domains encompassed all (FAD domain) and part (FMN domain) of the putative interdomain sequence. This interdomain sequence was identified by alignment of the amino acid sequence of MSR with that for rat CPR and by analysis of the crystallographic structure of rat CPR (*31*). The following oligonucleotide primers were used in PCR amplification: 5′ AAT GAA TTC GGC GCA CTC CCG GTG GCA TCAC 3′ (forward primer for the FAD domain incorporating an *Eco*RI restriction site), 5′ ATC CTC TTT CTT TAA TGC GGC CGC TTA TGA CCA AAT ATC CTG 3′ (reverse primer for the FAD domain which contains a *Not*I restriction site), 5′ CCG GAA TTC ATG CGC TTT CTG CTG CTG 3′ (forward primer for the FMN domain incorporating an *Eco*RI restriction site) and 5′ ATT CCA TAG CGG CCG CTC TTA GGG TAC CGA ACG GGT AAG TGA GGA 3′ (reverse primer for the FMN domain incorporating a *Not*I restriction site). The conditions used for PCR were denaturation at 94 °C for 2 min, followed by 30 cycles at 94 °C for 30 s, 52 °C for 30 s, and 72 °C for 2 min. The PCR products were digested with *Eco*RI and *Not*I and subcloned into pGEX-4-T1. The constructs were sequenced to ensure that no PCR-induced errors had been introduced and subsequently transformed into *E. coli* strain BL21(DE3) for the production of recombinant protein.

Expression and Purification of MSR and the Individual FAD and FMN Domains. Transformed cells of *E. coli* strain BL21(DE3) harboring the appropriate expression plasmid were grown overnight at 37 °C in LB media with 100 μg/mL ampicillin. The overnight culture (0.5 mL) was used to inoculate 0.5 L of modified Terrific broth (10 g of bactotryptone, 20 g of yeast extract, 4 mL of glycerol, 2.65 g of KH_2PO_4, and 4.33 g of Na_2HPO_4 per liter) containing 100 μg/mL ampicillin. The cultures were grown at 28 °C until the optical density at 600 nm reached a value of ∼1.0, and then isopropyl 1-thio-β-D-galactopyranoside to a final concentration of 0.1 mM was added. The cells were incubated for a further 12 h at 25 °C and were then harvested by centrifugation at 5000*g* for 25 min and stored at −80 °C.

The procedure for purifying MSR and the individual flavin domains was adapted from literature supplied by Novagen. The cell pellet was resuspended in buffer A (4.3 mM Na_2HPO_4, 1.47 mM KH_2PO_4, 0.137 M NaCl, 2.7 mM KCl, pH 7.3, 1 mM EDTA, 1 mM DTT) supplemented with Complete protease inhibitor tablets. The cells were lysed by the addition of 200 μg/mL lysozyme and by sonication (6 × 20 s pulses at 25% power with 3 min intervals using a Bandelin sonopuls GM2600). The lysate was centrifuged at 15000*g* for 50 min, and the supernatant was loaded onto a glutathione−Sepharose 4B column (75 × 39 mm) equilibrated with buffer A. The

column was washed with 3 L of buffer A. The chimeric protein, GST-MSR, was eluted with buffer B (50 mM Tris-HCl, pH 7.6, 1 mM DTT, 1 mM EDTA, and 10 mM glutathione). The GST tag was cleaved from MSR by incubation with thrombin at 4 °C, and MSR was dialyzed overnight against 50 mM potassium phosphate buffer, pH 7.0, to remove glutathione. The cleaved MSR was reapplied to a glutathione−Sepharose 4B column (54 × 30 mm) equilibrated with buffer A. MSR was separated from the remaining glutathione-binding proteins by washing the column with buffer A. MSR was dialyzed overnight in 50 mM potassium phosphate buffer, pH 7.0, at 4 °C. The protein was then purified further by anion-exchange chromatography on a Q-Sepharose high-performance column (145 × 25 mm) and eluted using a linear gradient ranging from 50 to 500 mM NaCl in 50 mM potassium phosphate buffer, pH 7.0, at a flow rate of 10 mL/min. The MSR fractions, as indicated by absorbance at 450 and 275 nm, were collected and concentrated by ultrafiltration. The protein was dialyzed against 50 mM potassium phosphate buffer, pH 7.0, followed by dialyses against 50 mM potassium phosphate buffer, pH 7.0, containing 50% glycerol, and stored at −80 °C. The FAD and FMN domains were also expressed, purified, and stored using the same purification protocol. The concentration of MSR, the FAD domain, and the FMN domain was determined by absorbance values at 450 nm with molar extinction coefficients of 25600, 11200, and 14700 M^{-1} cm^{-1}, respectively, using the spectroscopic method described in ref *32*.

Steady-State Reductase Assays. The rate of ferricyanide (FeCN) and cytochrome *c* reduction at 25 °C by MSR was determined by the change in absorbance at 420 nm (1020 M^{-1} cm^{-1}) and 550 nm (21100 M^{-1} cm^{-1}), respectively (*33*), on a Varian Cary 50 Bio UV−visible scanning spectrophotometer. The 1 mL reaction mixture contained 50 mM potassium phosphate buffer, pH 7.0, 1 mM FeCN or 60 μM cytochrome *c*, and 100 μM NADPH; the reaction was initiated by the addition of 1−2 μg of MSR. The apparent K_m for NADPH was determined with 60 μM cytochrome *c*, and NADPH was varied from 0.5 to 100 μM. The initial velocities obtained under varied NADPH concentrations were fitted to the Michaelis−Menten equation to obtain values for apparent V_{max} and apparent K_m.

Spectral Analysis. A Varian Cary 50 probe UV−visible spectrophotometer was used to record the absorbance spectra of oxidized MSR and the FAD- and FMN-binding domains. The CD spectra of the three proteins were recorded in the far-UV region on a Jasco J-720 spectrophotometer. The spectra were recorded in 50 mM potassium phosphate buffer, pH 7.0, at 25 °C.

Potentiometric Titrations. Redox titrations were performed in a Belle Technology glovebox maintained under a nitrogen atmosphere (oxygen maintained at <5 ppm) at 25 °C. The titration buffer, 100 mM potassium phosphate, pH 7.0, was made anaerobic by extensive bubbling with argon. Concentrated protein samples (0.1−0.5 mM) in a total volume of 1−2 mL were admitted to the glovebox and made oxygen free by filtering the sample over a 10 mL Bio-Rad Econo-Pac 10 DG column (15 × 60 mm) equilibrated with anaerobic titration buffer. The eluted protein was diluted to a final concentration of 25−100 μM with the titration buffer to a total volume of 10 mL. Solutions of the following redox mediators were added to the 10 mL protein solutions at micromolar final concentrations: benzyl viologen (1 μM), methyl viologen (0.5 μM; 0.3 μM for the isolated FAD domain), 2-hydroxy-1,4-naphthoquinone (5 μM), and phenazine methosulfate (2 μM). Absorption spectra from 280 to 800 nm were recorded using a fiber optic absorption probe (Varian) linked to a Varian Cary 50 probe UV−visible spectrophotometer. The electrochemical potential was monitored using a Hanna instruments pH211 pH/voltmeter coupled to Pt/calomel electrode (ThermoRussell Ltd.). The electrode was calibrated using the Fe(II)/Fe(III)-EDTA couple (+108 mV) as a standard. The oxidized protein was initially titrated to the reduced state with sodium dithionite and then reoxidized with potassium ferricyanide. After each addition of reductant or oxidant, the potential was recorded once it had stabilized at a fixed value, and the absorbance spectrum of the protein was taken. The observed potentials obtained with the platinum/calomel electrode were normalized to the standard hydrogen electrode by the addition of 244 mV to the potential values. A total of 30−80 spectra were collected at various potentials. During the titration of MSR, the absorbance between 700 and 800 nm increased by approximately 0.05 absorbance unit owing to baseline drift and a small amount of precipitation of the protein. All spectra were therefore corrected to the same baseline absorbance at 800 nm.

To determine the redox potentials for FAD and FMN, the absorbance of the flavin cofactors at various wavelengths during the titration was plotted against the potential. The absorbance at 600 nm, which is near the absorbance maxima for the blue neutral semiquinone, was the wavelength chosen to analyze the titration data for the individual FMN and FAD domains. The FMN domain titration data were also analyzed by plotting the oxidized absorbance maxima at 454 nm against the potential. The absorbance values between the wavelength ranges 450−460 nm and 580−605 nm were summed and plotted versus potential for the analysis of titration data for MSR. Finally, the absorbance values at 425 and 502 nm, isosbestic points revealed in the spectral titration of MSR, were plotted versus the potential. The titration data for the FAD and FMN domains were fitted to eq 1, which

$$A = \frac{a10^{(E-E'_1)/59} + b + c10^{(E'_2-E)/59}}{1 + 10^{(E-E'_1)/59} + 10^{(E'_2-E)/59}} \quad (1)$$

is derived by extension of the Beer−Lambert Law and the Nernst equation and describes a two-electron reduction process (*22*, *34*). Data for the titration of full-length MSR were fitted to eq 2, which represents the sum of two two-

$$A = \frac{a10^{(E-E'_1)/59} + b + c10^{(E'_2-E)/59}}{1 + 10^{(E-E'_1)/59} + 10^{(E'_2-E)/59}} + \frac{d10^{(E-E'_3)/59} + e + f10^{(E'_4-E)/59}}{1 + 10^{(E-E'_3)/59} + 10^{(E'_4-E)/59}} \quad (2)$$

electron redox processes. In these equations, *A* is the total absorbance, *a*, *b*, and *c* are the component absorbance values contributed by one flavin in the oxidized, semiquinone, and hydroquinone states, and *d*, *e*, and *f* are the component absorbance values corresponding to the second flavin in the oxidized, semiquinone, and hydroquinone states. *E* is the

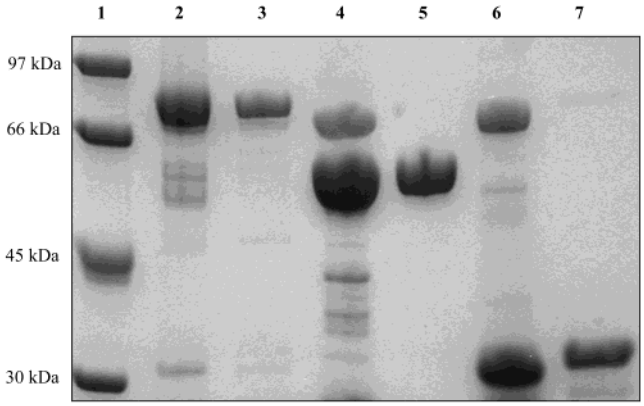

FIGURE 1: SDS−polyacrylamide gel electrophoresis analysis of the sequential purification of MSR and its component FAD- and FMN-binding domains from *E. coli*. Lanes: 1, molecular mass markers (97, 66, 45, and 30 kDa); 2, eluate from the glutathione−Sepharose 4B column following thrombin treatment of the *E. coli* lysate containing pGEXMSR; 3, pure MSR (77.7 kDa) obtained after Q-Sepharose anion-exchange chromatography of the eluate shown in lane 2; 4, as in lane 2, except the lysate was from *E. coli* containing the pGEXMSRFAD plasmid; 5, pure MSR FAD domain (59.4 kDa) obtained after Q-Sepharose anion-exchange chromatography of the eluate shown in lane 4; 6, as in lane 2, except the lysate was from *E. coli* containing the pGEXMSRFMN plasmid; 7, pure MSR FMN domain (27.1 kDa) obtained after Q-Sepharose anion-exchange chromatography of the eluate shown in lane 6.

observed potential; E'_1 and E'_2 are the midpoint potentials for the ox/sq and sq/hq couples, respectively, for the first flavin, and E'_3 and E'_4 are the corresponding midpoint potentials for the second flavin.

A fit of the absorbance versus potential data for the isolated FAD and FMN domains to eq 1 by nonlinear least-squares regression analysis using Origin (version 6.0) software (Microcal) yielded the midpoint potentials for the ox/sq and sq/hq couples. The redox titration data for MSR were fitted using eq 2. However, owing to the large number of parameters in fitting to eq 2, estimates of the potential values (parameters $E'_1-E'_4$) were entered and fixed, using data gathered from the fits for the isolated FAD/NADPH and FMN domains to provide the initial estimates for the flavin potentials. After several iterations reasonable estimates of the individual flavin absorbance values (parameters $a-f$) were obtained. These absorbance values were then fixed, and potential values were then allowed to vary during the fitting routine. This process was repeated several times, allowing the potential values to vary in the final fitting session.

RESULTS

Protein Purification, Spectral Properties, and Catalytic Activity. Recombinant human MSR and its component FAD- and FMN-binding domains were expressed in *E. coli* as GST fusion proteins, permitting purification by glutathione affinity chromatography (Figure 1). After cleavage of the GST tag with thrombin and separation from the other glutathione-binding proteins, MSR and the FAD and FMN domains were further purified by anion-exchange chromatography. The apparent molecular masses of purified MSR, the FAD domain, and the FMN domain are 78, 60, and 30 kDa, respectively. These values are in close agreement with values calculated from the amino acid sequences of MSR (77.7 kDa), the FAD domain (59.4 kDa), and the FMN domain (27.1 kDa).

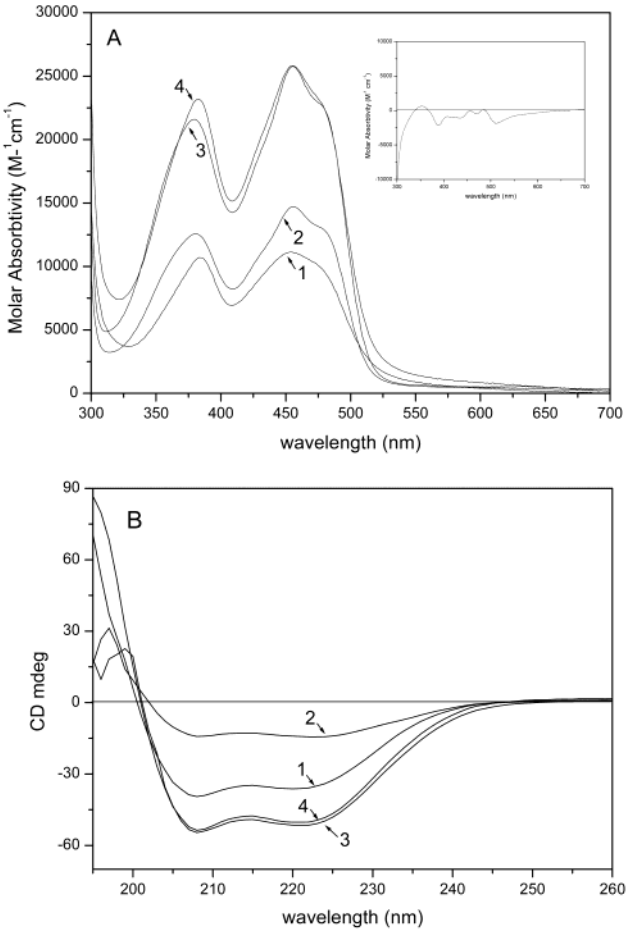

FIGURE 2: Spectra of MSR and the MSR FAD- and MSR FMN-binding domains. Panel A: Absorbance spectra of the fully oxidized (1) MSR FAD domain, (2) MSR FMN domain (3), and full-length MSR and (4) the addition of the spectra for the MSR FAD domain and MSR FMN domain (1 + 2). Inset: difference spectrum generated by subtraction of the spectrum of full-length MSR from that of the summed spectra of the two MSR flavin domains (3 − 4). Panel B: Far-UV CD spectra of (1) the FMN domain (6 μM), (2) the FAD domain (6 μM), and (3) MSR (6 μM) and (4) the addition of the individual spectra (1 + 2) of the isolated flavin-binding domains.

The ability of the FAD and FMN cofactors to retain similar redox properties in their respective isolated domains and in the full-length MSR was observed during purification of the three proteins. In the first chromatographic step, the fraction containing the FMN domain was grayish blue, indicating that the flavin was in the partially reduced blue semiquinone state. In contrast, FAD was in the fully oxidized state, as the FAD domain component was yellow throughout the purification. The green color of full-length MSR in the initial stages of purification thus likely reflects a mixture of blue semiquinone FMN and yellow fully oxidized FAD components. A similar phenomenon has been observed for human CPR (*22*).

The absorbance spectra of fully oxidized MSR and the isolated domains are shown in Figure 2A. The FMN domain and full-length MSR show typical flavin absorbance spectra with peaks at 380 and 454 nm and a shoulder at 474 nm (*2*, *35*). The fully oxidized FAD domain has absorbance peaks at 382 and 454 nm. The summed absorbance spectra of the FAD and FMN domains closely mimic that of full-length

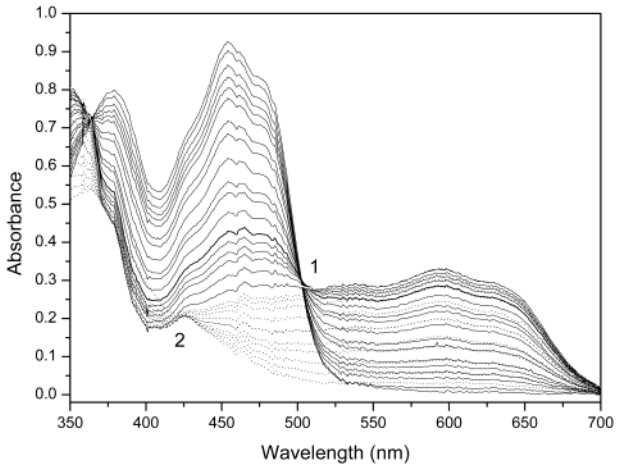

FIGURE 3: Absorption spectra for the redox titration of the FMN domain of human MSR (63 μM). The spectra were obtained after each addition of dithionite as described in the Experimental Procedures. The solid lines demark spectra recorded during the addition of the first electron and as such follow the transition of FMN from the oxidized to the semiquinone state. An isosbestic point appearing at 501 nm is indicated by "1". The dotted lines are spectra taken during the addition of the second reducing equivalent and thus show the flavin's semiquinone to hydroquinone transition. A second isosbestic point, denoted by "2", appears in this phase at 425 nm. The spectral properties of the FMN domain overlapped closely during titrations in both oxidative and reductive directions.

MSR; however, the absorbance peak at 380 nm for MSR has shifted by 2 nm to 382 nm in the additive spectrum and increased in intensity. This difference in absorbance profiles may indicate a change in solvent exposure or the amino acid geometry around the flavins in the full-length enzyme versus the isolated domains.

To investigate if separation of the domains induced secondary structural changes in the proteins, the far-UV CD spectra were measured of MSR and the isolated domains (Figure 2B). The far-UV spectra of the isolated domains could be added together to generate a spectrum that mimics that of the intact enzyme and that of a stoichiometric mixture of the two domains. This suggests that the domains retain their secondary structure as isolated components.

Like CPR and the reductase domain of NOS, MSR is able to catalyze the NADPH-dependent reduction of cytochrome *c* and FeCN (*2*, *20*, *21*). The apparent steady-state turnover rates for MSR determined under the conditions described in the Experimental Procedures are 0.8 s^{-1} and 8.7 s^{-1} for cytochrome *c* and FeCN reduction, respectively, at 25 °C. The apparent K_m for NADPH, with cytochrome *c* as the terminal electron acceptor, is 4.0 ± 0.3 μM. The values obtained for the rate of cytochrome *c* reduction and the K_m for NADPH are similar to those reported previously (*2*). The reductase activities are between 25- and 100-fold lower than those reported for CPR (*21*) and NOS (*20*).

Redox Titration of the FMN Domain. The absorbance spectrum of the FMN domain throughout the course of the redox titration is shown in Figure 3. The protein remained soluble and stable during the titration, permitting good quality sets of spectra to be obtained. The addition of the first reducing equivalent converts FMN from the oxidized to the blue neutral semiquinone form, and this is represented spectrally (solid lines in Figure 3) with the appearance of a broad absorbance band with a maximum at 597 nm and a

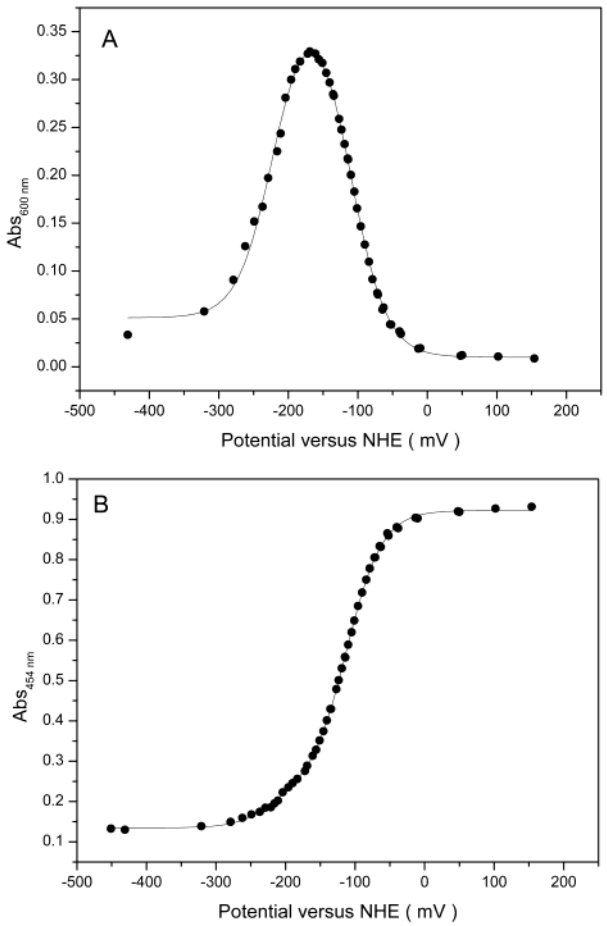

FIGURE 4: Plots of absorbance at 600 nm (panel A) and at 454 nm (panel B) versus potential for the FMN domain of MSR. Both data sets were fitted to eq 1, and the resultant values for the redox potentials for the ox/sq and sq/hq couples for FMN are shown in Table 1.

decrease in absorbance at 454 nm. The dotted lines in Figure 3 represent the spectral intermediates of the FMN domain as it converts from the semiquinone to the hydroquinone form following further addition of dithionite. During this phase both absorbance bands at 450 and 597 nm are lost. Clear isosbestic points are observed for the ox/sq transition at 502 nm and for the sq/hq transition at 427 nm. Panels A and B of Figure 4 show the dependence of absorbance values at 600 and 454 nm on the reduction potential, respectively. The data shown in these plots were fitted to eq 1, and the midpoint potentials determined from both sets were identical, within error. The FMN ox/sq couple is −112 mV while the FMN sq/hq is −221 mV (Table 1). The difference in the potentials of the two couples is approximately 110 mV, explaining the large semiquinone signal that accumulates on reduction by dithionite. The semiquinone formed is the neutral, blue (protonated) form, as observed in EPR studies with full-length MSR (*19*) and with other eukaryotic diflavin reductases (*22*, *27*).

Redox Titration of the FAD Domain. Spectra of the FAD domain during redox titration with dithionite are shown in Figure 5. The protein remained relatively stable during the titration, although the last few additions of dithionite needed to fully reduce the cofactor caused a small amount of precipitation, as evident by a small drift in the absorbance between 700 and 800 nm. Consequently, the last few data

Table 1: Reduction Potentials for the Flavin Cofactors in Methionine Synthase Reductase

	reduction potential (mV) vs normal hydrogen electrode			
	FMN cofactor		FAD cofactor	
protein	ox/sq	sq/hq	ox/sq	sq/hq
FMN domain	-112 ± 1[a]	-221 ± 2		
FAD domain			-222 ± 4	-288 ± 7
MSR (450)[b]	-109 ± 1	-227 ± 10	-254 ± 5	-291 ± 8
MSR (600)[c]	-106 ± 1	-213 ± 9	-224 ± 31	-279 ± 6
MSR (iso)[d]	-107 ± 1	-217 ± 4	-257 ± 5	-281 ± 8

[a] The errors are from nonlinear least-squares fitting of the data shown in the corresponding figure. The midpoint potentials determined from separate experiments ($n = 3$) for the isolated FMN domain, isolated FAD domain, and full-length MSR (determined from data fitting at 450 nm and at isosbestic points) vary by 6−15 mV, the largest variation being observed for MSR. [b] Values are from a fit of eq 2 to the data shown in Figure 8A. [c] Values are from a fit of eq 2 to the data shown in Figure 8B. [d] Values are from a fit of eq 1 to the data shown in Figure 9.

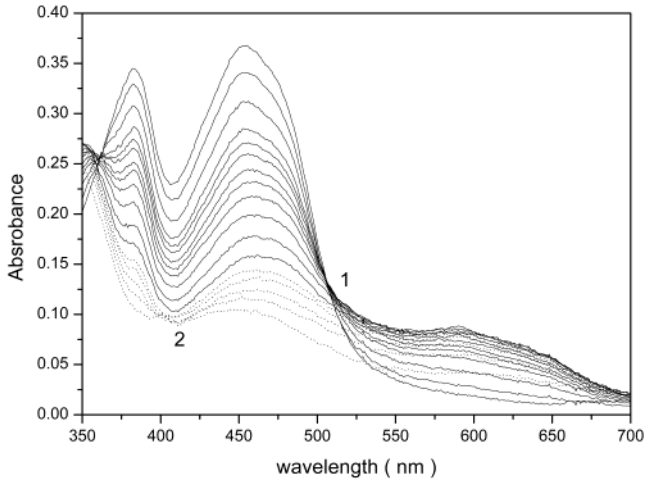

FIGURE 5: Absorption spectra for the redox titration of the FAD domain for MSR (33 μM). The spectra were obtained after each addition of dithionite as described in the Experimental Procedures. The solid lines demark spectra recorded during the addition of the first electron and as such follow the transition of FAD from the oxidized to the semiquinone state. An isosbestic point appearing at 502 nm is indicated by "1". The dotted lines are spectra taken during the addition of the second reducing equivalent and thus show the flavin's semiquinone to hydroquinone transition. A second isosbestic point, denoted by "2", appears in this phase at 415 nm. As with the FMN domain, the FAD domain was reoxidized fully by titration with FeCN, and the spectra matched that of the initial reductive titration.

points were omitted in the fitting routine. Notwithstanding the small amount of aggregation observed at low redox potentials, the FAD domain of MSR exhibits greater solubility in this regime by comparison with the FAD domains of CPR (*22*), NR1 (*30*), and P450 BM3 (*36*). The additional amino acid residues encompassing the hinge region of MSR included in the construct encoding the isolated FAD domain might endow the protein with improved solubility.

The initial addition of dithionite causes the absorbance maxima at 454 nm to decrease concomitant with an increase in absorbance at 589 nm. The latter absorbance change signifies the formation of a blue neutral semiquinone. During this phase of the redox titration, represented spectrally with solid lines in Figure 5, FAD is converted from the oxidized

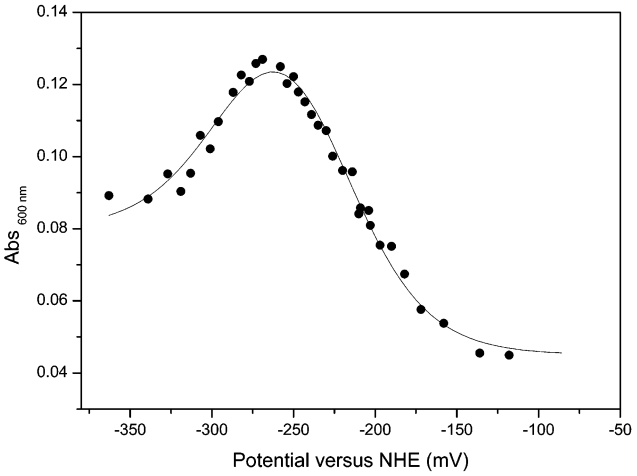

FIGURE 6: Plot of absorbance at 600 nm versus potential for the FAD domain of MSR. Data were fitted to eq 1, and the determined values for the redox potentials for the ox/sq and sq/hq couples for FAD are shown in Table 1.

to the semiquinone state. As the second reducing equivalent is added, both absorbance maxima at 454 and 589 nm decrease as FAD semiquinone is reduced further to the hydroquinone (dotted lines in Figure 5). The isosbestic points for the ox/sq transition and the sq/hq transition appear at 506 and 417 nm, respectively. The absorbance at 600 nm was plotted against the redox potential (Figure 6), and the data were fitted to eq 1. The midpoint potentials of the FAD ox/sq and sq/hq couples are −222 and −288 mV, respectively (Table 1). Approximately 60−70 mV separates the two couples, which again facilitates formation of a thermodynamically stable blue semiquinone on the FAD.

Redox Titration of Full-Length MSR. Titration of full-length MSR with dithionite is accompanied by a small amount of protein precipitation, indicated by a drift in absorbance at 800 nm of approximately 0.05 absorbance unit between the first and last spectrum recorded. Before data analysis, the absorbances at 800 nm of individual spectra were corrected to compensate for this drift. Figure 7 shows the corrected spectral changes during redox titration for full-length MSR. During the first phase of the titration (solid lines in Figure 7), the addition of dithionite enables the formation of a blue neutral semiquinone species, indicated by the increase in absorbance at 594 nm. In this phase of the titration, at a reduction potential above −140 mV, an isosbestic point is present at 502 nm, attributed to the FMN ox/sq transition. In the second phase of the titration (dotted lines in Figure 7), from potential values of −140 to −240 mV, the semiquinone signal at 594 nm remains close to its maximal absorbance while the absorbance values at shorter wavelengths decrease. Isosbestic points are absent during this phase of the titration as multiple partially reduced forms of MSR exist, which are inferred to be the FMN sq/FAD ox, FMN sq/FAD sq, FMN hq/FAD sq forms. In the third and final phase of the redox titration (dashed lines in Figure 7), at potentials more negative than −250 mV, the semiquinone signal decreases concomitantly with a further decrease in absorbance at 450 nm. A second isosbestic point appears during this phase at 425 nm, reflecting the transition of FAD sq to FAD hq.

A plot of the summed absorbance between 450 and 460 nm (across the oxidized flavin absorbance maximum of

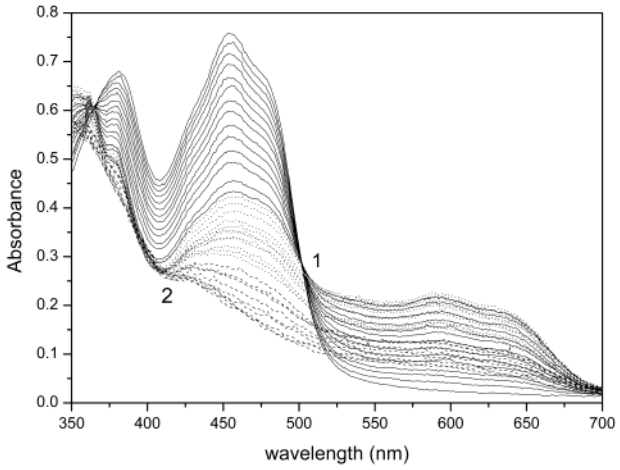

FIGURE 7: Absorption spectra for the redox titration of MSR (29 μM). The spectra were collected after each addition of dithionite as described in the Experimental Procedures. The solid lines demark spectra recorded during the addition of the first electron and as such follow the transition of the flavins from the oxidized to the semiquinone state. An isosbestic point at 502 nm appearing during this transition is indicated by "1". The dotted lines indicate spectra recorded between approximately −140 and −240 mV. The dashed lines indicate spectra at potentials more negative than −240 mV, where an isosbestic point at 425 nm, denoted by "2", appears.

MSR) versus potential is shown (Figure 8A). The redox profile can be divided approximately into two regions, which merge at approximately −140 mV. Previous potentiometric analysis with related diflavin reductases (*22*) suggests that the region at the positive end of the plot describes the FMN ox/sq couple, while the region at the negative end of the plot is a function of the three remaining redox couples: FAD ox/sq, FAD sq/hq, and FMN sq/hq. Corresponding plots for redox titrations performed with NOS (*27*) and CPR (*22*) show a larger separation between the two sigmoidal-like regions. This suggests either a greater difference between the values for the FMN ox/sq couple and those for the remaining three redox couples or an altered order of the low-potential couples in MSR compared to CPR and/or NOS. In the plots for NOS and CPR, there is a clear "plateau" region between the two phases of absorbance change. A plot of the summed absorbance between 580 and 605 nm (across the blue semiquinone maxima) versus the potential is also shown (Figure 8B). The right-hand side of the bell-shaped curve describes the high-potential FMN ox/sq couple, while the left-hand side of the curve encompasses the titration of the remaining three couples. The corresponding plots for NOS (*27*) and CPR (*22*) describe two superimposed, asymmetric bell-shaped curves, for which the overlap region details absorbance changes associated with the FMN sq/hq and FAD ox/sq transitions. These features are not distinguished in the plot for MSR, again indicating that there should be differences in separation and/or order of the redox couples of CPR and NOS. The data for the redox titration of MSR were fitted to eq 2, which relates the change in absorbance and potential to a four-electron reduction process. However, owing to the large number of parameters (10 in total), constraints were imposed in the fitting process (described in the Experimental Procedures) to obtain reasonable estimates of the values for the four redox couples. Furthermore, the close values of the redox couples in the low-potential region (i.e., the lack of inflections or shoulders in Figure 8) likely influence the

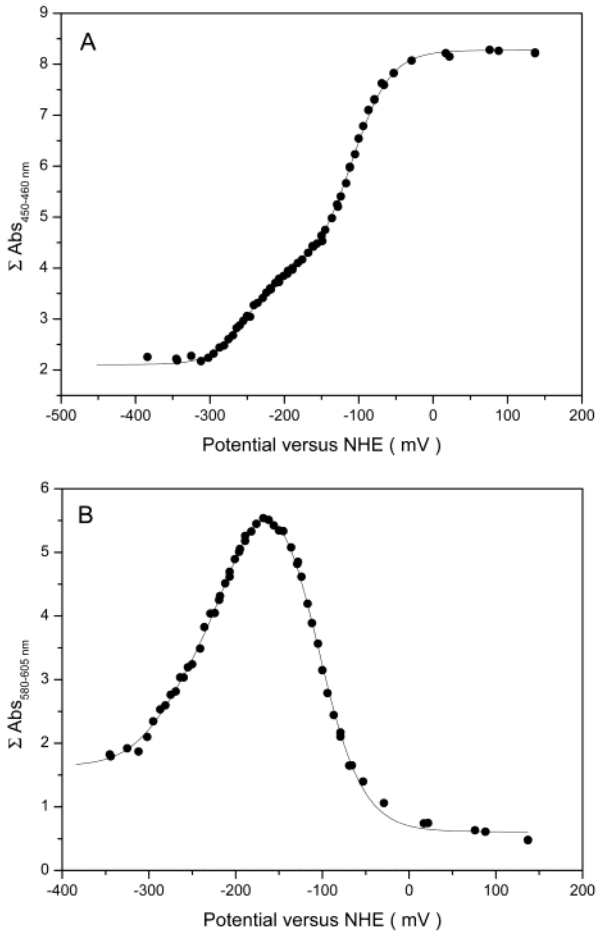

FIGURE 8: Absorbance versus potential plots for MSR. In panel A, the absorbance values between 450 and 460 nm are summed together and plotted against the reduction potential. In panel B, the summed absorbance values between 580 and 605 nm are plotted against the reduction potential. Both data sets were fitted to eq 2, described in the Experimental Procedures, and the redox potentials for the ox/sq and sq/hq couples for the two flavins determined from the spectra are shown in Table 1.

ability of the fitting process to obtain meaningful values for the redox couples without fixing the absorbance values.

The redox titration data for full-length MSR were further analyzed by plotting the isosbestic points at 425 and 502 nm versus the measured potential (panels A and B of Figure 9, respectively). At an isosbestic point there is a near-zero absorbance change occurring with the electronic transition of a redox couple, the ox/sq transition in the case of the isosbestic point at 502 nm. Thus, a plot of absorbance change at this wavelength (502 nm) versus potential can be used to determine the midpoint potentials of the sq/hq couples for each of the flavins. Conversely, a plot of absorbance at 425 nm versus potential can be used to determine the midpoint potentials of the ox/sq couples for each of the flavins. The data in Figure 9 were fitted to eq 1, and the calculated midpoint potentials for the four couples were as follows: FMN ox/sq = −107 mV,; FMN sq/hq = −217 mV, FAD ox/sq = −257 mV, and FAD sq/hq = −281 mV (Table 1).

DISCUSSION

Methionine is an essential amino acid in mammals as it is required for protein synthesis as well as having a central

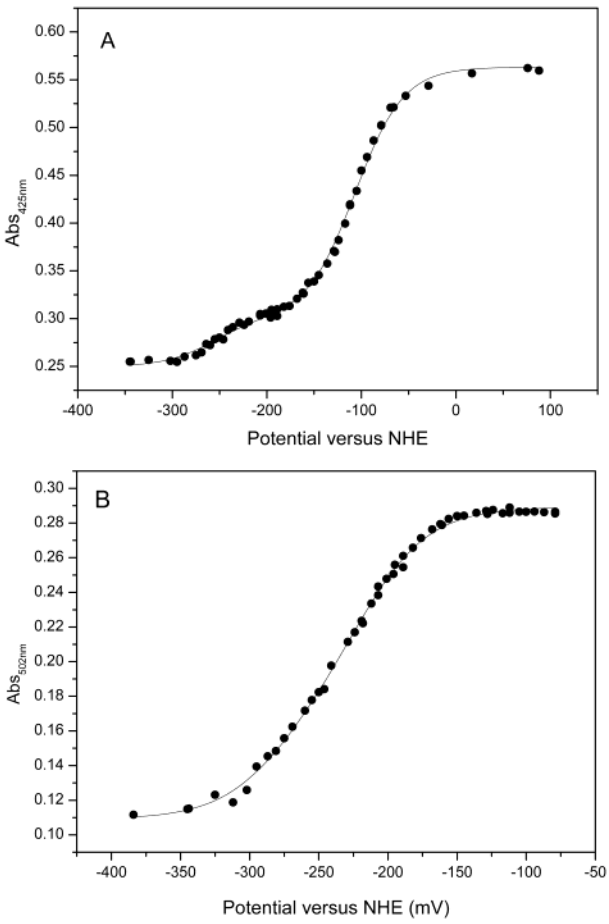

FIGURE 9: Absorbance versus potential plots for MSR at isosbestic points shown in Figure 7. Panel A shows a plot of absorbance at 425 nm, the approximate isosbestic point for the ox/sq couple of both flavins, against the potential. Panel B shows a plot of absorbance at 502 nm, the approximate isosbestic point for the sq/hq couples of both flavins, against the potential. The data were fitted to eq 1, as described in the Experimental Procedures, and the midpoint potentials for all four couples are shown in Table 1.

role in one-carbon metabolism. Impairment of methionine synthesis leads to megaloblastic anemia, hyperhomocysteinemia, homocystinuria, and hypomethioninemia (*10*, *12*). Afflicted patients can exhibit a variety of symptoms including developmental delay, neonatal seizures, and blindness (*11*). The hereditary basis for the physiological conditions in these patients has been linked to polymorphisms in genes encoding MS, MSR, and methylenetetrahydrofolate reductase (*10*, *12*, *37*). Mutations in these genes presumably impair the function of the respective protein and subsequent ability of the cell to convert homocysteine to methionine. The specific toxic effects of elevated levels of homocysteine in the blood plasma are not known, but the condition leads to an increased risk of mothers bearing children with neural tube defects (*15*, *16*) or Down's syndrome (*17*) and of cardiovascular disease (*13*, *38*, *39*) and Alzheimer's disease in adults (*40*). Recent cloning of the gene for MSR has led to the identification of clinically relevant mutations located in both conserved and nonconserved regions (*1*, *41*, *42*). Through studies documenting the occurrence of polymorphisms in several defined populations, particular mutations in the gene have been linked to premature coronary heart disease (*43*), spina bifida (*42*), and Down's syndrome (*17*, *44*). Thus, it is of particular

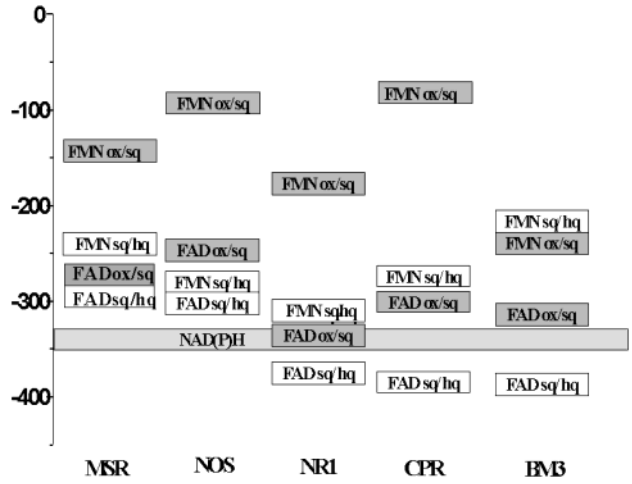

FIGURE 10: Flavin reduction potentials for members of the diflavin reductase family. The various midpoint potentials for the ox/sq (gray boxes) and sq/hq couples (white boxes) of the FAD and FMN cofactors for MSR, NOS, NR1, CPR, and flavocytochrome P450 BM3 are shown. The midpoint reduction potential of NADP(H) (−320 mV) is shown as a dotted bar.

interest to investigate the thermodynamic and kinetic properties of MSR to establish how these clinically relevant mutations potentially affect the behavior of the enzyme.

This paper is the first investigative study into the thermodynamic behavior of MSR, reporting on the redox potentials of the FAD and FMN cofactors. To assist in the assignment of the high- and low-potential flavins, MSR was genetically dissected into its component FAD and FMN domains. Constructs encoding the individual component domains and intact MSR were generated to express the proteins in *E. coli*. The purified proteins show flavin absorbance spectra typical of related flavoproteins (*2*, *23*). Anaerobic redox titration of the individual domains established that both flavins populate a neutral, blue semiquinone species and have midpoint reduction potentials within the ranges found for other characterized diflavin reductase enzymes. The redox-dependent absorbance changes and flavin reduction potentials determined from analysis of the flavin domains were then used to help to determine the four corresponding couples in full-length MSR.

The individual MSR FAD/NADPH and FMN polypeptides retained secondary structural properties typical of their domains in the full-length enzyme. The minor difference between the far-UV CD spectrum of intact MSR and that obtained by addition of the spectra for the domains (at identical concentration) may result from the fact that there is a small overlap region of polypeptide shared by both of the domains (Figure 2B). However, the combined absorbance of the FAD and FMN domains did not overlap precisely with that of full-length MSR. The shift in the absorbance intensity and peak at 380 nm suggests that domain dissection may induce minor changes in environment of one or both flavins, possibly increasing cofactor solvent accessibility.

The midpoint potentials for the MSR FAD and FMN cofactors fall within the spectrum shown for NOS, CPR, and NR1; the four redox couples are more closely compressed than those of the three other human diflavin enzymes (Figure 10). All four couples in the enzymes shown appear to be poised in similar fashion, with the FMN ox/sq couple being

considerably more positive than the other three couples. Only in NOS does the overall order of the couples differ, with the FAD ox/sq couple being more positive than the FMN sq/hq couple (*27*). In NOS and CPR, the flavins are considered to cycle between the one- and three-electron reduced states during catalysis (*45*, *46*). Similar to rabbit CPR (*23*), the FMN ox/sq couple in MSR lies at −110 mV, approximately 50−60 mV more negative than human CPR, NOS, and P450 BM3 and 30 mV more positive than NR1 (*22*, *27*, *36*). A relatively small separation (<50 mV) exists between the FMN sq/hq and the FAD ox/sq couple for all four human diflavin enzymes. Finally, the MSR FAD sq/hq couple, like NOS, is more positive than the midpoint potential for NADP(H) (−320 mV), while the corresponding potential for human CPR and NR1 is 40−60 mV more negative than this value. While there is considerable overlap in the overall set of redox couples in the human diflavin enzymes, each reductase has evolved to have its own unique set of redox couples, likely geared to the catalytic requirements of the system.

The thermodynamic properties of MSR suggest that the mechanism of electron transfer is similar to that of the related diflavin enzymes. Once hydride is transferred from NADPH to the oxidized FAD cofactor, there is a disproportionation of electrons between the flavins. The equilibrium favors the FMN cofactor as the FMNox/sq couple is 100 mV more positive than the remaining three couples. This likely disfavors reverse electron/hydride transfer to $NADP^+$, an event which occurs physiologically with FNR and has been demonstrated with CPR (*26*). One electron is then transferred from FMN to MS for reduction of the cob(II)alamin cofactor. The fate of the second reducing equivalent has yet to be determined.

Future work will involve expanding these studies to investigate the effects of clinically relevant mutations of MSR on the thermodynamic properties of the flavin cofactors and on the steady-state and stopped-flow kinetic behavior of the enzyme. The steady-state reductase activity of MSR is slow compared to its homologues CPR and NOS, and this study indicates that this phenomenon is not rooted in adverse thermodynamic barriers to catalysis. Thus, key structural differences between MSR, CPR, NR1, and NOS may mediate reduction rates of electron transfer to these artificial electron acceptors. The extended interdomain linker region in MSR might contribute to altered rates of internal electron transfer and rates of electron transfer from flavins to exogenous electron acceptors. This reinforces the importance of obtaining structural data for this medically important enzyme, and we are currently pursuing this approach.

REFERENCES

1. Leclerc, D., Wilson, A., Dumas, R., Gafuik, C., Song, D., Watkins, D., Heng, H. H., Rommens, J. M., Scherer, S. W., Rosenblatt, D. S., and Gravel, R. A. (1998) *Proc. Natl. Acad. Sci. U.S.A. 95*, 3059−3064.
2. Olteanu, H., and Banerjee, R. (2001) *J. Biol. Chem. 276*, 35558−35563.
3. Ludwig, M. L., and Matthews, R. G. (1997) *Annu. Rev. Biochem. 66*, 269−313.
4. Drennan, C. L., Huang, S., Drummond, J. T., Matthews, R. G., and Ludwig, M. L. (1994) *Science 266*, 1669−1674.
5. Fujii, K., Galivan, J. H., and Huennekens, F. M. (1977) *Arch. Biochem. Biophys. 178*, 662−670.
6. Bianchi, V., Reichard, P., Eliasson, R., Pontis, E., Krook, M., Jornvall, H., and Haggard-Lungquist, E. (1993) *J. Bacteriol. 175*, 1590−1595.
7. Porter, T., and Kasper, C. (1985) *Proc. Natl. Acad. Sci. U.S.A. 82*, 973−977.
8. Bredt, D. S., Hwang, P. M., Glatt, C. E., Lowenstein, C., Reed, R. R., and Snyder, S. H. (1991) *Nature 351*, 714−718.
9. Paine, M. J., Garner, A. P., Powell, D., Sibbald, J., Sales, M., Pratt, N., Smith, T., Tew, D. G., and Wolf, C. R. (2000) *J. Biol. Chem. 275*, 1471−1478.
10. Harding, C. O., Arnold, G., Barness, L. A., Wolff, J. A., and Rosenblatt, D. S. (1997) *Am. J. Med. Genet. 71*, 384−390.
11. Watkins, D., and Rosenblatt, D. S. (1988) *J. Clin. Invest. 81*, 1690−1694.
12. Watkins, D., and Rosenblatt, D. S. (1989) *Am. J. Med. Genet. 43*, 427−434.
13. Refsum, H., Ueland, P. M., Nygard, O., and Vollset, S. E. (1998) *Annu. Rev. Med. 49*, 31−62.
14. Masser, P. A., Taylor, L. M. J., and Porter, J. M. (1994) *Ann. Thorac. Surg. 58*, 1240−1246.
15. Steegers-Theunissen, R. P., Boers, G. H., Trijbels, F. J., Finkelstein, J. D., Blom, H. J., Thomas, C. M., Borm, G. F., Wouters, M. G., and Eskes, T. K. (1994) *Metabolism 43*, 1475−1480.
16. Mills, J. L., McPartlin, J. M., Kirke, P. N., Lee, Y. J., Conley, M. R., Weir, D. G., and Scott, J. M. (1995) *Lancet 345*, 149−151.
17. O'Leary, V. B., Parle-McDermott, A., Molloy, A. M., Kirke, P. N., Johnson, Z., Conley, M., Scott, J. M., and Mills, J. L. (2002) *Am. J. Med. Genet. 15*, 107−111.
18. Leclerc, D., Campeau, E., Goyette, P., Adjalla, C. E., Christensen, B., Ross, M., Eydoux, P., Rosenblatt, D. S., Rozen, R., and Gravel, R. A. (1996) *Hum. Mol. Genet. 5*, 1867−1874.
19. Olteanu, H., Munson, T., and Banerjee, R. (2002) *Biochemisrty 41*, 13378−13385.
20. Sheta, E. A., McMillian, K., and Masters, B. S. S. (1994) *J. Biol. Chem. 269*, 15147−15153.
21. Shen, A. L., and Kasper, C. B. (2000) *J. Biol. Chem. 275*, 41087−41091.
22. Munro, A., Noble, M. A., Robledo, L., Daff, S. N., and Chapman, S. K. (2001) *Biochemistry 40*, 1956−1963.
23. Iyanagi, T., Makino, N., and Mason, H. S. (1974) *Biochemistry 13*, 1701−1710.
24. Vermilion, J. L., and Coon, M. L. (1978) *J. Biol. Chem. 253*, 8812−8819.
25. Oprian, D. D., and Coon, M. J. (1982) *J. Biol. Chem. 257*, 8935−8944.
26. Gutierrez, A., Lian, L.-Y., Wolf, C. R., Scrutton, N. S., and Roberts, G. C. K. (2001) *Biochemistry 40*, 1964−1967.
27. Noble, M. A., Munro, A. W., Rivers, S. L., Robledo, L., Daff, S. N., Yellowlees, L. J., Shimizu, T., Sagami, I., Guillemette, J. G., and Chapman, S. K. (1999) *Biochemistry 38*, 16413−16418.
28. Miller, R. T., Martasek, P., Omura, T., and Masters, B. S. S. (1999) *Biochem. Biophys. Res. Commun. 265*, 184−188.
29. Knight, K., and Scrutton, N. S. (2002) *Biochem. J. 367*, 19−30.
30. Finn, R. D., Basran, J., Roitel, O., Wolf, C. R., Munro, A. W., Paine, M. J. I., and Scrutton, N. S. (2003) *Eur. J. Biochem.* (in press).
31. Wang, M., Roberts, D. L., Paschke, R., Shea, T. M., Masters, B. S., and Kim, J. J. (1997) *Proc. Natl. Acad. Sci. U.S.A. 94*, 8411−8416.
32. Macherox, P., Ed. (1999) *Flavoprotein Protocols. Methods in Molecular Biology* (Chapman, S. K., and Reid, G. A., Eds.) Vol. 131, pp 4−5, Humana Press, Totowa, NJ.
33. Gelder, B. F. V., and Slater, E. C. (1962) *Biochim. Biophys. Acta 58*, 593−595.
34. Dutton, P. L. (1978) *Methods Enzymol 54*, 411−435.
35. Smith, G. C., Tew, D. G., and Wolf, C. R. (1994) *Proc. Natl. Acad. Sci. U.S.A. 91*, 8701−8714.
36. Daff, S. N., Chapman, S. K., Turner, K. L., Holt, R. A., Govindaraj, S., Poulos, T. L., and Munro, A. W. (1997) *Biochemistry 36*, 13816−13823.
37. Gulati, S., Baker, P., Li, Y. N., Fowler, B., Kruger, W., Brody, L. C., and Banerjee, R. (1996) *Hum. Mol. Genet. 5*, 1859−1865.
38. Brattstrom, L., Israelsson, B., and Hultberg, B. (1992) *Lakartidningen 89*, 467−469.
39. Kang, S. S., Wong, P. W., and Malinow, M. R. (1992) *Annu. Rev. Nutr. 12*, 279−298.

40. Seshardi, S., Beiser, A., Selhub, J., Jacques, P. F., Rosenberg, I. H., D'Agostino, R. B., Wilson, P. W., and Wolf, P. A. (2002) *N. Engl. J. Med. 346*, 476−483.
41. Wilson, A., Leclerc, D., Rosenblatt, D. S., and Gravel, R. A. (1999) *Hum. Mol. Genet. 8*, 2009−2016.
42. Wilson, A., Platt, R., Wu, Q., Leclerc, D., Christensen, B., Yang, H., Gravel, R. A., and Rozen, R. (1999) *Mol. Genet. Metab. 67*, 317−323.
43. Brown, C. A., McKinney, K. Q., Kaufman, J. S., Gravel, R. A., and Rozen, R. (2000) *J. Cardiovasc. Risk 7*, 197−200.
44. Hobbs, C. A., Sherman, S. L., Yi, P., Hopkins, S. E., Torfs, C. P., Hine, R. J., Pogribna, M., Rozen, R., and James, S. J. (2000) *Am. J. Med. Genet. 107*, 151−155.
45. Gachhui, R., Presta, A., Bentley, D. F., Abu-Soud, H. M., McArthur, R., Brudvig, G., Ghosh, D. K., and Stuehr, D. J. (1996) *J. Biol. Chem. 271*, 20594−20602.
46. Vermillion, J. L., Balloou, D. P., Massey, V., and Coon, M. J. (1981) *J. Biol. Chem. 256*, 266−277.

BI027290B